Electronic band gaps and exciton binding energies in monolayer Mo_{x}W_{1-x}S_{2} transition metal dichalcogenide alloys probed by scanning tunneling and optical spectroscopy

Albert F. Rigosi, Heather M. Hill, Kwang Taeg Rim, George W. Flynn, and Tony F. Heinz

Phys. Rev. B **94**, 075440 — Published 29 August 2016

DOI: 10.1103/PhysRevB.94.075440

Electronic band gaps and exciton binding energies in monolayer $Mo_xW_{1-x}S_2$ transition metal dichalcogenide alloys probed by scanning tunneling and optical spectroscopy

Albert F. Rigosi[1,3], Heather M. Hill[1,3], Kwang Taeg Rim[2], George W. Flynn[2], and Tony F. Heinz[1,3*]

[1]*Departments of Physics and Electrical Engineering, Columbia University, 538 West 120th St., New York, NY 10027, United States*

[2]*Department of Chemistry, Columbia University, 500 West 120th St., New York, NY 10027, United States*

[3]*Department of Applied Physics, Stanford University, 348 Via Pueblo Mall, Stanford, CA 94305, United States*
and SLAC National Accelerator Laboratory, 2575 Sand Hill Road, Menlo Park, CA 94025, United States

(Received 2 April 2016;)

ABSTRACT: Using scanning tunneling spectroscopy (STS) and optical reflectance contrast measurements, we examine band-gap properties of single layers of transition metal dichalcogenide (TMDC) alloys: MoS_2, $Mo_{0.5}W_{0.5}S_2$, $Mo_{0.25}W_{0.75}S_2$, $Mo_{0.1}W_{0.9}S_2$, and WS_2. The quasi-particle band gap, spin-orbit separation of the excitonic transitions at the K/K' point in the Brillouin zone, and binding energies of the A exciton are extracted from STS and optical data. The exciton binding energies change roughly linearly with tungsten concentration. For our samples on an insulating substrate, we report quasi-particle band gaps from 2.17 ± 0.04 eV (MoS_2) to 2.38 ± 0.06 eV (WS_2), with A exciton binding energies ranging from 310 to 420 meV.

PACS numbers: 74.55.+v, 71.35.Cc, 73.22.-f

I. INTRODUCTION

Atomically thin, two-dimensional (2D) materials such as graphene and transition metal dichalcogenides (TMDCs) have been the focus of much recent interest. The TMDCs exhibit phenomena ranging from an indirect-to-direct band gap transition in the monolayer limit [1-8], efficient light-matter interactions [9-14], strong coupling of the valley and spin degrees of freedom [15-19], and pronounced many-body effects [20-22]. The basic electronic properties of TMDC monolayers, including their band gaps and exciton binding energies, have also been the subject of recent studies [23-27]. In addition to these fundamental materials investigations, many promising electronic and optoelectronic device concepts have been explored based on TMDC monolayer materials [28-29].

An important possibility for the TMDC family is the use of alloys to continuously tune the band gap of the material between the stoichiometric end points. Monolayer TMDC alloys have already been investigated both theoretically [30-31] and experimentally [32-39]. In particular, $Mo_{1-x}W_xS_2$ monolayers, the subject of the present paper, were investigated both optical and electrically by Chen *et al.* [40-41]. While this work demonstrated the appreciable tunability of the optical band gap as a function of composition in the alloy, the variation the exciton binding energy or, equivalently, of the quasi-particle band gap with composition was not directly addressed. In view of exciton binding energies of hundreds of meV, the distinction between the optical band gap and the quasi-particle band gap must be borne in mind, and the variation of the exciton binding energy is potential significant.

In the present work, we further investigate the $Mo_{1-x}W_xS_2$ monolayer alloys using two complementary experimental techniques, one optical and one electrical, to obtain information about the optical and quasi-particle band gaps and, by comparison, of the exciton binding energy. The principal optical measurement is reflection contrast spectroscopy, which yields the absorption spectrum of the sample and, hence, very directly, the optical band gap or exciton transition energy. This approach is similar to measurement of the photoluminescence spectrum, but is less perturbed by the potential influence of defect states. The measurement of the optical contrast spectra also allow us to clearly identify the higher-lying spin-orbit split B exciton (in addition to the band-edge A exciton) [20,42] and thus to track the energy separation of these two states as a function of alloy composition. The electrical technique employed to obtain the quasi-particle band gap is scanning tunneling spectroscopy, under of conditions of tunneling both into and out of the sample. Analysis of the tunneling spectra reveals information about the energy of the band edges of the conduction and valence bands and, hence, the quasi-particle band gap of the material. A similar method of measuring the quasi-particle band gap using scanning tunneling spectroscopy was utilized by Ugeda *et al.* [43] for a different TMDC system. In our study, we perform detailed characterization of the two stoichiometric compounds and three alloys in the $Mo_{1-x}W_xS_2$ family: MoS_2, $Mo_{0.5}W_{0.5}S_2$, $Mo_{0.25}W_{0.75}S_2$, $Mo_{0.1}W_{0.9}S_2$, and WS_2.

II. EXPERIMENTAL METHODS

A. Sample Preparation

We prepared TMDC samples on fused quartz substrates using mechanical exfoliation of stoichiometric and alloyed bulk crystals from a commercial supplier (2D Semiconductors). The exfoliated monolayers were identified by means of photoluminescence (PL) and Raman

spectroscopy, as well as atomic force microscopy (AFM) (see Supplementary Material) [44]. The PL spectra were compatible with previously reported results for the corresponding monolayer alloy [40-41]. While the use of a transparent substrate was helpful for precise analysis of the reflection contrast spectra, as discussed below, for the scanning tunneling microscopy (STM) measurements, we needed further processing to make electrical contact to the samples. This was accomplished by evaporating a metal contact using a shadow mask. The use of a shadow mask allowed us to avoid the sample degradation that is often encountered in conventional lithographic processing. Further information about sample preparation for the STM measurements is provided in the Supplementary Material [44].

B. Reflectance Contrast Measurements

For the reflectance contrast measurements, the broadband emission from a tungsten halogen lamp was spatially filtered by a pinhole and then focused onto the sample to a spot size of about 2 μm using a 40x objective. The reflected light was collected by the same objected and analyzed with a spectrometer equipped with liquid-nitrogen-cooled CCD camera. All measurements on the alloyed samples were performed at room temperature.

The reflectance contrast, $\Delta R/R$, is given by the difference in the reflectance of the substrate with and without the TMDC monolayer normalized by the reflectance of the bare substrate: $\Delta R/R = (R\text{-}R_0)/R_0$, where R is the reflection from the substrate with the sample and R_0 is the reflection from the bare fused quartz substrate. For transparent substrates and relatively small values of $\Delta R/R$, the reflectance contrast is proportional to the absorption of the TMDC layer, with a constant of proportionality determined by the known substrate refractive index [45]. In the

analysis below, we present both the measured $\Delta R/R$ spectra and the corresponding absorption of the monolayer.

C. Scanning Tunneling Microscopy and Spectroscopy Measurements

Both STM and STS measurements were conducted at room temperature on a commercial instrument (Omicron VT) with a tungsten tip [46-48]. Each sample was annealed in the STM chamber under ultrahigh vacuum (UHV) at 450 K for two hours prior to performing the measurements. The constant current mode was used to collect all STM images, with a tunneling voltage of V = +1.5 Volts.

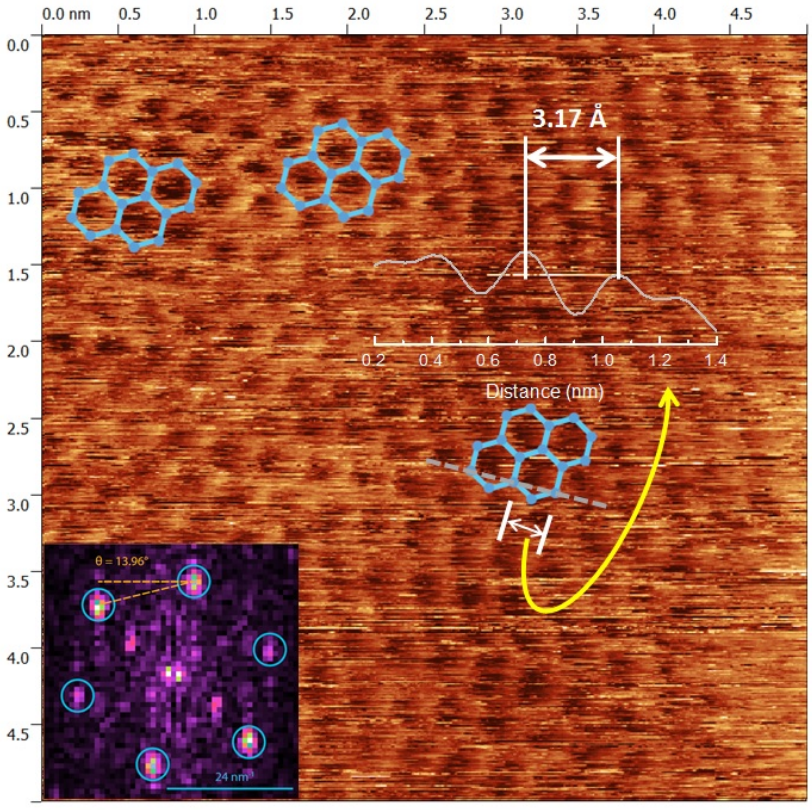

FIG. 1. (Color online) STM topography image for a $Mo_{0.5}W_{0.5}S_2$ monolayer (5 nm x 5 nm area, V = +1.5 V, I = 100 pA). The TMDC lattice structure (light blue) is superimposed as a guide to

the eye. A topography scan along the dotted grey line matches the expected lattice period. The Fourier transform of the real-space image (lower left) displays the expected periodicity.

A typical STM image of a monolayer of $Mo_{0.5}W_{0.5}S_2$ is presented in Figure 1. It reveals the expected structure and periodicity. The electronic structure of the monolayer alloys was probed by STS measurements. The spectra were collected by turning off the feedback for the tip height and recording the tunneling current *I* while quickly ramping the tunneling voltage *V*. The process was repeated, after reactivating the feedback mechanism, at different spatial locations on the sample to improve the signal-to-noise ratio. The resulting averaged *I-V* curves were numerically differentiated to obtain *dI/dV* spectra, which we present and discuss in this paper.

III. EXPERIMENTAL RESULTS

A. Reflectance Contrast Spectra

The measured reflectance contrast spectra of the stoichiometric and alloyed monolayers are presented in Fig. 2. We also present the corresponding optical absorption of the monolayers, inferred from the reflectance contrast spectra using the relation described above [45]. The two strong peaks in the spectra are the A and B excitonic transitions, which arise from the spin-split bands at the K and K' points of the Brillouin zone. The energy difference of the A and B excitons is attributed mostly from the valence band splitting [19,49-50]. As can be seen in Fig. 2 and summarized in Table 1, the A exciton transition energy increases monotonically with W concentration. In addition, the A-B energy separation increases significantly with increasing W concentration (also summarized in Table 1), reflecting the stronger spin-orbit interaction of the heavier element W compared with the lighter element Mo.

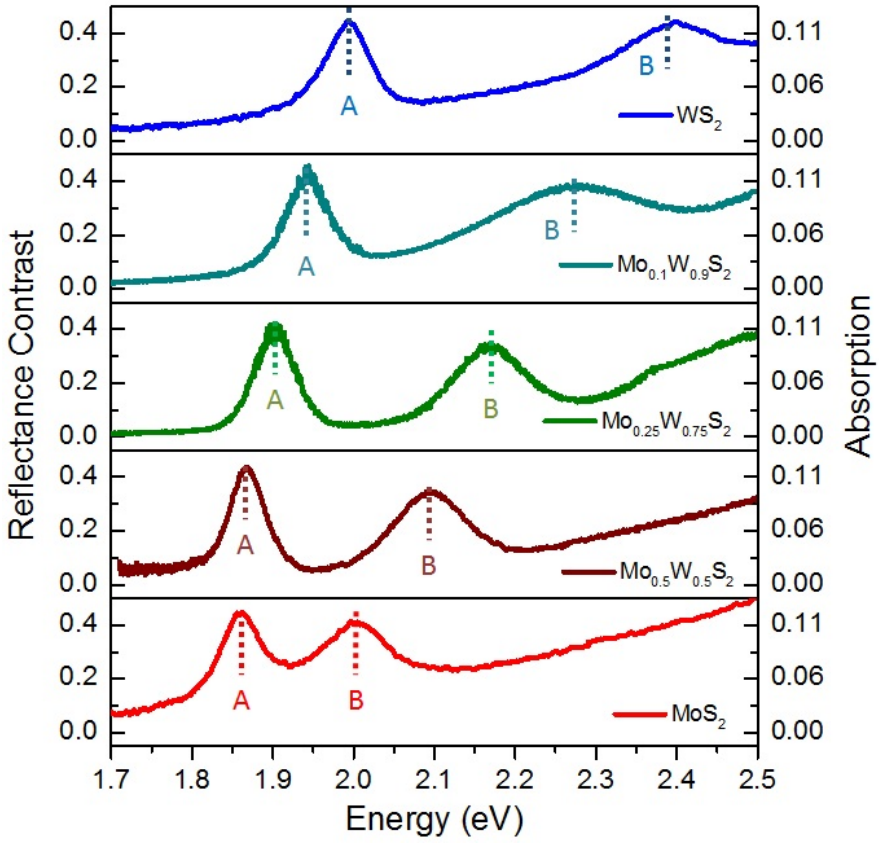

FIG. 2. (Color Online) Reflectance contrast spectra (left vertical scale) and optical absorption (right scale) for monolayers of the three indicated $Mo_{1-x}W_xS_2$ alloys and two stoichiometric end compounds. The transition energies of the A and B excitons, indicated by dotted lines in the figure, are summarized in Table 1.

B. Scanning Tunneling Spectroscopy

In Fig. 3 we present the *dI/dV* spectra for the five different samples over a voltage range from -2V to +2V. For each sample, we collected eighty sets of STS data. To assess the reproducibility of the data, randomly selected subsets of data were averaged and are compared in Figure 3. The variation among the different spectra is indicative of the reproducibility of the measurements.

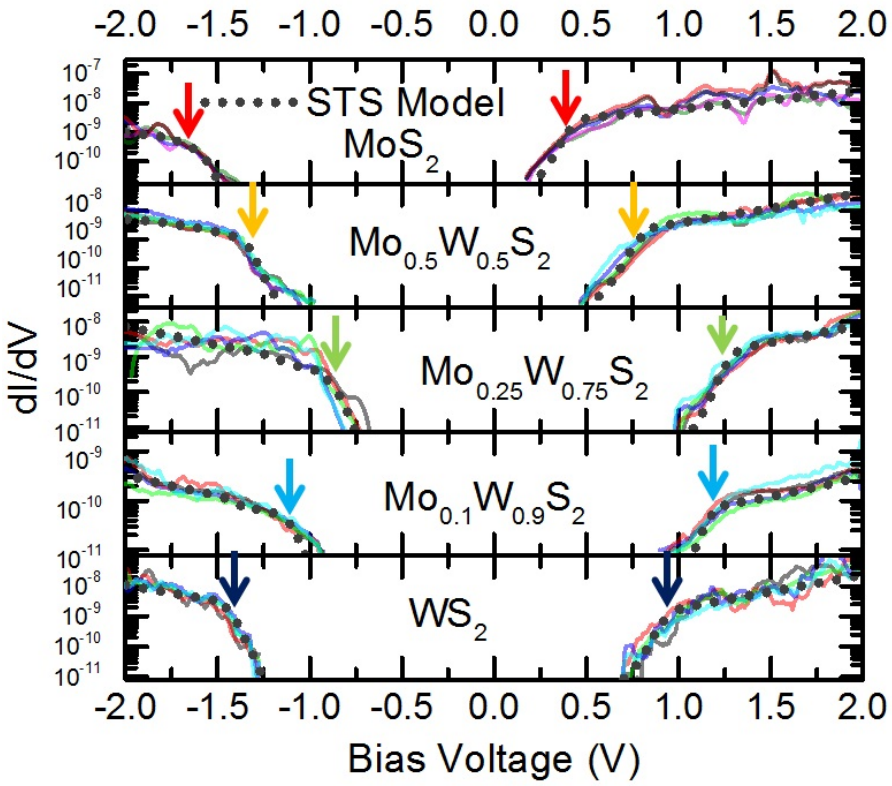

FIG. 3. (Color online) *dI/dV* spectra from the STS measurements of the $Mo_{1-x}W_xS_2$ alloys and stoichiometric monolayers. Each of the solid curves is an average of 16 randomly selected data sets. The dotted lines are fits to the model described in the text. The locations of the band edges are indicated by the arrows.

IV. DISCUSSION

A. Model for Tunneling Spectra

Our primary aim in analyzing the scanning tunneling spectra is to extract the quasi-particle band gap for each of the different TMDC alloy monolayers. While the band gap corresponds roughly to the region where we observe negligible tunneling current, to determine a reliable value for the band gap from the experimental data, we need to develop a model for the variation in tunneling current with tip bias. Here we describe tunneling from different regions in the

Brillouin zone of a 2D electronic band, as well as the influence of the finite (300 K) measurement temperature.

The tunneling current from a given band in the solid can be expressed as [51]:

$$I = \frac{4\pi e}{\hbar}\int_{-\infty}^{\infty}\left[\frac{1}{1+e^{\frac{\varepsilon-eV}{kT}}}-\frac{1}{1+e^{\frac{\varepsilon}{kT}}}\right]\rho_S\left(E_F-eV+\varepsilon\right)\rho_T\left(E_F+\varepsilon\right)T\left(z,V\right)d\varepsilon \quad (1)$$

where E_F is the Fermi energy, kT is the thermal energy, and V is the tunneling voltage, as above. The term in brackets accounts for the effect of finite temperature in the tip and sample. The tunneling current depends on the local density of states (LDOS) of the sample ρ_S and tip ρ_T, as well as the tunneling probability $T(z,V)$ for tip height z and tunneling voltage V. (See Supplementary Material for additional details.) We describe the tunneling probability by a simple model [52]:

$$T \sim e^{-2z\sqrt{\frac{2m}{\hbar^2}\left(\frac{\Phi_s+\Phi_t}{2}-\frac{|eV|}{2}+E\right)}} \quad (2)$$

where Φ_s and Φ_t are the work functions of the sample and tip, respectively, and m is the free electron mass. Here $E=\frac{\hbar^2 k_{\|}^2}{2m^*}$ is the energy associated with the in-plane motion of an electron with in-plane momentum $k_{\|}$ and effective mass m^*, which is assumed to dominate the tunneling process. This term is included to describe electron tunneling from the sample away from the center of the Brillouin zone, relevant for tunneling from K/K' point for the TMDC monolayers. This treatment of role of parallel momentum in the tunneling probability was also implemented in another recent work [52].

B. Determination of Quasi-Particle Band Gaps from STS Data

Using the model described above, we have fit the experimental dI/dV spectra for the five different sample compositions under study. In these simulations, the tip LDOS is assumed to be a constant, while the LDOS of the sample is a step function appropriate for a 2D parabolic band. In the expression for the tunneling probability T, we use Φ_s = 5.1 eV (work function of monolayer MoS_2) [53-54] or 5.8 eV (work function of monolayer WS_2) [55], and Φ_t = 4.5 eV (work function of tungsten metal tip). We assume that tunneling is dominated by the behavior at the K/K' points the Brillouin zone and consequently use $k_{\parallel} \approx 1.33 \text{Å}^{-1}$ [56]. The effective masses of the electrons (m*) are taken as $0.35m$ and $0.3m$ for MoS2 and WS2, respectively [57]. Parameters for the alloyed samples were assumed to vary linearly with composition between MoS_2 and WS_2. The initial tip-to-sample distance was taken to be z = 5 Å.

As can be seen from the results in Fig. 3, we are able to obtain a good fit to the experimental data using this simple model. The key adjustable parameters in the fits are the energies for the quasi-particle band gaps. Although it is a relatively small correction for most tunneling voltages, we have included not only the upper valence band, but also the lower, spin-orbit split band, with a separation determined by the experimental A-B exciton energy splitting. The fits shown in Fig. 3 are based on least-squares regressions, as described in detail in the Supplementary Material.

In obtaining an accurate value for the quasi-particle band gaps, we also need to account for the modest effect of the tip in perturbing charge state of the sample by tip-induced band bending (TIBB) in the 2D layer. As discussed in detail in the Supplementary Materials, we have evaluated TIBB by means of a simulation tool developed by R. Feenstra (SEMITIP v6) [58-60]. An important parameter in determining the degree of TIBB is the charge density in the

monolayer. We have assumed a carrier density of 2 x 10^{12} cm^{-2}, based on measurements of monolayer WS_2 after an annealing step [61]. The expected amount of TIBB, including bending of both the VB and CB, is ~30 meV. This value must be subtracted from the quasi-particle band gap inferred from the STS spectra.

From this analysis, we obtain values for the valence and conduction band edges, the difference of which yields the quasi-particle band gaps. The results are shown in Table 1 (and Figure 4) for both the stoichiometric compounds and the $Mo_{1-x}W_xS_2$ alloys. The quasi-particle band gaps of the MoS_2 and WS_2 monolayer were found to be 2.17 ± 0.04 eV and 2.38 ± 0.06, respectively. These values lie in the range of quasi-particle band gaps reported by other researchers for MoS_2 and WS_2 [43, 62-64]. For the alloys, we see a monotonic variation with composition between the two end stoichiometric compounds (Table 1 and represented graphically in Figure 4).

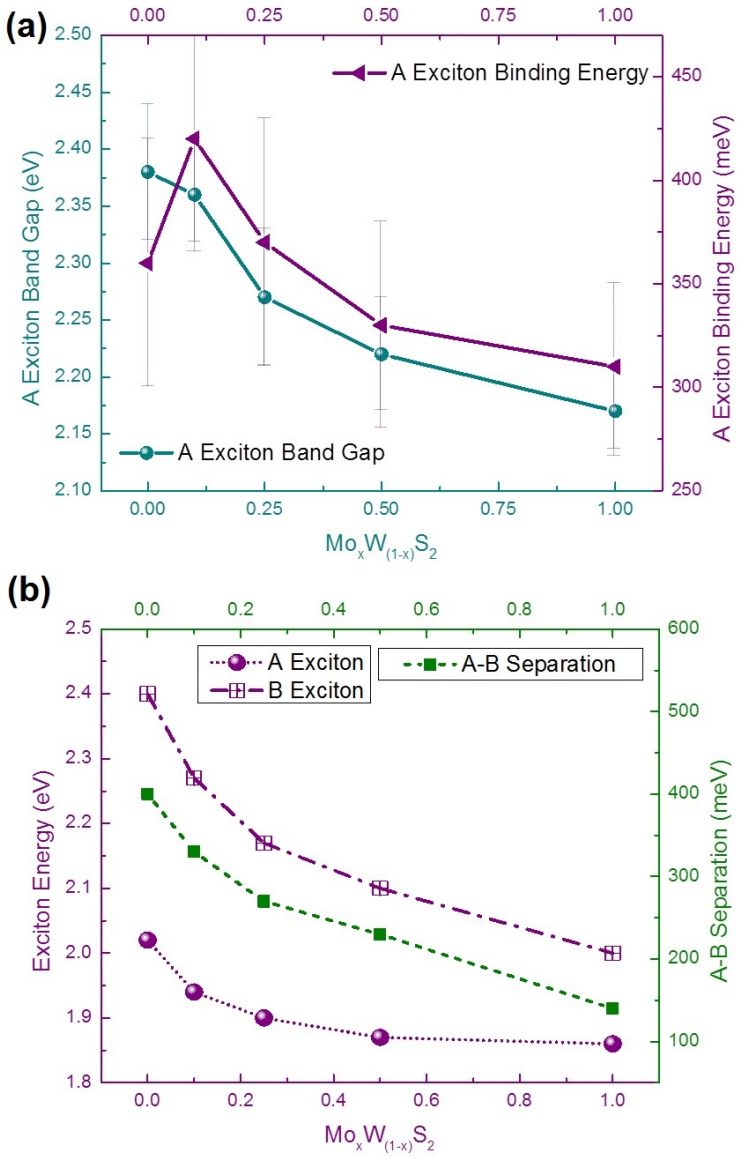

FIG. 4. (Color online) (a) The quasi-particle band gap and A exciton binding energies, which required the STS and reflectance contrast data to be inferred, are presented in blue and purple, respectively. (b) The energy of the A and B exciton and the A-B separation is shown here as a purple sphere, purple square, and green curve, respectively. The A-B separation is caused by spin-orbit coupling and varies semi-linearly with tungsten concentration.

Before leaving the interpretation of the quasi-particle band gap deduced from the STS data, we wish to comment on the assumption made above that the gap inferred from these measurements corresponds to that at the K point of the Brillouin zone. In particular, because the tunneling probability decreases with increasing later momentum of the carriers, as indicated in Eqn. (2), tunneling from other parts of the Brillouin zone may be favored over tunneling into or out of states at the K points, even if the latter has the lowest energy, and might, in principle, dominate the tunnel spectra. In particular, for the CB of MoS_2, the Q point (between K and Γ) has the next lowest energy after the K point [28,65-66], about 250 meV higher in energy [52]. If we interpret the measured STS gap of 2.17 eV as occurring to the Q point of the CB, then the gap to the K point around 1.92 eV. Comparing this energy to the measured A exciton transition energy of 1.86 eV, we would then infer an exciton binding energy in monolayer MoS_2 below 100 meV. This small exciton binding energy is incompatible with generally expected monolayer TMDC binding energies from previous experiments [23-27]. We therefore conclude that under our experimental conditions we are measuring the direct quasi-particle band gap at the K point. This interpretation is consistent with previously reported results [60].

C. Variation of Measured Quantities with Alloy Composition

In Table 1 and Figure 4 we present both the quasi-particle band gaps inferred for the five $Mo_{1-x}W_xS_2$ monolayers and the corresponding A exciton transition energies inferred from the reflection contrast measurements. Comparing these values immediately yields the exciton binding energies for the family of samples. There is an overall trend for the exciton binding energy to increase with tungsten concentration, yielding 310 ± 40 meV and 360 ± 50 meV for MoS_2 and WS_2, respectively. Previous optical studies have revealed comparable or larger values [23-27,67-68]. For the case of MoS_2, binding energies in this range are to be expected when the

effective environmental dielectric screening is approximately 2 [69]. For the case of WS_2, our room temperature value falls within the uncertainty of previously measured [23,25].

The trends in band gap trends with alloy composition are in agreement with density functional theory calculations presented in [40]. However, the trend for the binding energies is found to possibly have non-monotonic behavior, with a decrease in the exciton binding energy from $Mo_{0.1}W_{0.9}S_2$ to WS_2. This behavior may reflect variations in the effective masses of the carriers [31,70].

TABLE I. Values of the alloy band gaps (including TIBB effects), A exciton and its binding energy (including TIBB effects), B exciton, and A-B exciton separation.

Material:	MoS_2	$Mo_{0.5}W_{0.5}S_2$	$Mo_{0.25}W_{0.75}S_2$	$Mo_{0.1}W_{0.9}S_2$	WS_2
Band gap (eV):	**2.17 ± 0.04**	**2.20 ± 0.06**	**2.27 ± 0.06**	**2.36 ± 0.06**	**2.38 ± 0.06**
A exciton energy (eV)	**1.86**	**1.87**	**1.90**	**1.94**	**2.02**
B exciton energy (eV)	**2.00**	**2.10**	**2.17**	**2.27**	**2.40**
Binding energy (meV)	**310 ± 40**	**330 ± 50**	**370 ± 60**	**420 ± 50**	**360 ± 60**
A-B splitting (meV)	**140**	**230**	**270**	**330**	**400**

V. CONCLUSIONS

In conclusion, we studied the optical response of MoS_2, $Mo_{0.5}W_{0.5}S_2$, $Mo_{0.25}W_{0.75}S_2$, $Mo_{0.1}W_{0.9}S_2$, and WS_2 over a spectral range of 1.7 – 2.5 eV using reflectance spectroscopy, and examined the behavior of the band gap of each of the materials using scanning tunneling spectroscopy. We find that a number of the properties of the TMDC alloys are dependent on the concentration of the transition metal, including the position of the A and B exciton, the A-B separation energy as it reflects the nature of the spin-orbit coupling, the band gap, and the A exciton binding energies.

ACKNOWLEDGMENTS

The authors acknowledge the National Science Foundation for support through grant DMR-1123894. A.R. and H.M.H. acknowledge funding from the National Science Foundation through the Graduate Research Fellowship Program (DGE-1144155) and the Integrated Graduate Education and Research Training Fellowship (DGE-1069240), respectively. The authors would like to thank Tingyi Gu, Randall Feenstra, Xiaodong Zhou, Alexey Chernikov, and Abhay Pasupathy for fruitful discussions.

TABLE OF CONTENTS GRAPHIC (END OF DOC)

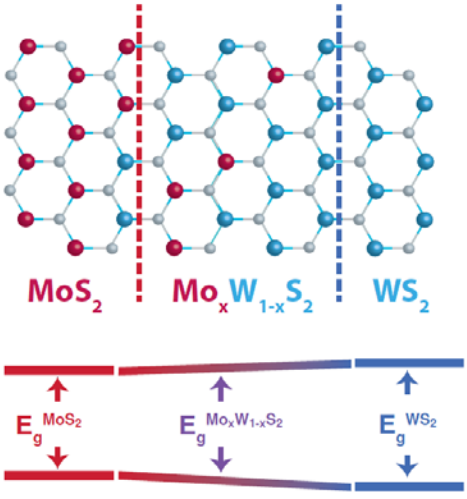

REFERENCES

[1] K. S. Novoselov, D. Jiang, F. Schedin, T. J. Booth, V. V. Khotkevich, S. V. Morozov, and A. K. Geim, Proc. Natl. Acad. Sci. U.S.A. **102**, 10451 (2005).

[2] S. Das, J. A. Robinson, M. Dubey, H. Terrones, and M. Terrones, Annu. Rev. of Mater. Sci. **45**, 1 (2015).

[3] S. Z. Butler, S. M. Hollen, L. Cao, Y. Cui, J. A. Gupta, H. R. Gutiérrez, T. F. Heinz, S. S. Hong, J. Huang, A. F. Ismach, E. Johnston-Halperin, M. Kuno, V. V. Plashnitsa, R. D. Robinson, R. S. Ruoff, S. Salahuddin, J. Shan, L. Shi, M. G. Spencer, M. Terrones, W. Windl, and J. E. Goldberger, ACS Nano **7**, 2898– 2926 (2013).

[4] P. Tonndorf, R. Schmidt, P. Bottger, X. Zhang, J. Borner, A. Liebig, M. Albrecht, C. Kloc, O. Gordan, and D. R. T. Zahn, et al, Opt. Express **21**, 4908– 4916 (2013).

[5] K. F. Mak, C. Lee, J. Hone, J. Shan, and T. F. Heinz, Phys. Rev. Lett. **105**, 136805 (2010).

[6] M. Chhowalla, H. S. Shin, G. Eda, L. J. Li, K. P. Loh, and H. Zhang, Nat. Chem. **5**, 263– 275 (2013).

[7] H. Li, G. Lu, Y. L. Wang, Z. Y. Yin, C. X. Cong, Q. Y. He, L. Wang, F. Ding, T. Yu, and H. Zhang, Small **9**, 1974– 1981 (2013).

[8] J. A. Wilson, and A. D. Yoffe, Adv. Phys. **18**, 193– 335 (1969).

[9] A. Splendiani, L. Sun, Y. Zhang, T. Li, J. Kim, C. Chim, G. Galli, and F. Wang, Nano Lett. **10**, 1271– 5 (2010).

[10] C. Ruppert, O. B. Aslan, and T. F. Heinz, Nano Lett. **14**, 6231 (2014).

[11] W. Zhao, Z. Ghorannevis, L. Chu, M. Toh, C. Kloc, P. Tan, and G. Eda, ACS Nano **7**, 791– 797 (2013).

[12] G. Eda, H. Yamaguchi, D. Voiry, T. Fujita, M. Chen, and M. Chhowalla, Nano Lett. **11**, 5111– 5116 (2011).

[13] M. Bernardi, M. Palummo, and J. C. Grossman, Nano Lett. **13**, 3664– 3670 (2013).

[14] Y. Li, A. Chernikov, X. Zhang, A. Rigosi, H. M. Hill, A. M. van der Zande, D. A. Chenet, E.-M. Shih, J. Hone, and T. F. Heinz, Phys. Rev. B **90**, 205422 (2014).

[15] K. F. Mak, K. He, J. Shan, and T. F. Heinz, Nat. Nanotechnol. **7**, 494– 498 (2012).

[16] D. Xiao, G.-B. Liu, W. Feng, X. Xu, and W. Yao, Phys. Rev. Lett. **108**, 196802 (2012).

[17] K. F. Mak, K. L. McGill, J. Park, and P. L. McEuen, Science **344**, 1489– 1492 (2014).

[18] X. Xu, W. Yao, D. Xiao, and T. F. Heinz, Nat. Phys. **10**, 343– 350 (2014).

[19] G. Wang, C. Robert, A. Suslu, B. Chen, S. Yang, S. Alamdari, I. C. Gerber, T. Amand, X. Marie, S. Tongay, and B Urbaszek, Nat. Commun. **6**, 10110 (2015).

[20] D. Y. Qiu, F. H. da Jornada, and S. G. Louie, Phys. Rev. Lett. **111**, 216805 (2013).

[21] T. C. Berkelbach, M. S. Hybertsen, and D. R. Reichman, Phys. Rev. B **88**, 045318 (2013).

[22] G. Moody, C. K. Dass, K. Hao, C.-H. Chen, L.-J. Li, A. Singh, K. Tran, G. Clark, X. Xu, G. Berghuser, E. Malic, A. Knorr, X. Li, Nat. Commun. **6**, 8315 (2015).

[23] H. M. Hill, A. F. Rigosi, C. Roquelet, A. Chernikov, T. C. Berkelbach, D. R. Reichman, M. S. Hybertsen, L. E. Brus, and T. F. Heinz, Nano Lett. **15**, 2992 (2015).

[24] B. Zhu, X. Chen, and X. Cui, Sci. Rep. **5**, 9218 (2015).

[25] A. Chernikov, T. C. Berkelbach, H. M. Hill, A. Rigosi, Y. Li, O. B. Aslan, D. R. Reichman, M. S. Hybertsen, and T. F. Heinz, Phys. Rev. Lett. **113**, 076802 (2014).

[26] A. T. Hanbicki, M. Currie, G. Kioseoglou, A. L. Friedman, and B. T. Jonker, Solid State Commun. **203**, 16 (2015).

[27] Z. Ye, T. Cao, K. O'Brien, H. Zhu, X. Yin, Y. Wang, S. G. Louie, and X. Zhang, Nature **513**, 214 (2014).

[28] Q. Wang, K. Kalantar-Zadeh, A. Kis, J. N. Coleman, M. S. Strano, Nat. Nanotechnol. **7**, 699-712 (2012).

[29] D. Jariwala, V. K. Sangwan, L. J. Lauhon, T. J. Marks, and M. C. Hersam, ACS Nano **8**, 1102– 1120 (2014).

[30] H. P. Komsa, and A. V. Krasheninnikov, J. Phys. Chem. Lett. **3**, 3652– 3656 (2012).

[31] J. Y. Xi, T. Q. Zhao, D. Wang, and Z. G. Shuai, J. Phys. Chem. Lett. **5**, 285– 291 (2014).

[32] D. O. Dumcenco, H. Kobayashi, Z. Liu, Y.-S. Huang, and K. Suenaga, Nat. Commun. **4**, 1351 (2013).

[33] H. Li, X. Duan, X. Wu, X. Zhuang, H. Zhou, Q. Zhang, X. Zhu, W. Hu, P. Ren, P. Guo, L. Ma, X. Fan, X. Wang, J. Xu, A. Pan, and X. Duan, J. Am. Chem. Soc. **136**, 3756–3759 (2014).

[34] Q. Ma, M. Isarraraz, C. S. Wang, E. Preciado, V. Klee, S. Bobek, K. Yamaguchi, E. Li, P. M. Odenthal, and A. Nguyen, et al, ACS Nano **8**, 4672– 4677 (2014).

[35] S. Tongay, D. S. Narang, J. Kang, W. Fan, C. H. Ko, A. V. Luce, K. X. Wang, J. Suh, K. D. Patel, and V. M. Pathak, et al, Appl. Phys. Lett. **104**, 012101 (2014).

[36] J. Mann, Q. Ma, P. M. Odenthal, M. Isarraraz, D. Le, E. Preciado, D. Barroso, K. Yamaguchi, G. von Son Palacio, and A. Nguyen, et al, Adv. Mater. **26**, 1939 (2014).

[37] M. Zhang, J. Wu, Y. Zhu, D. O. Dumcenco, J. Hong, N. Mao, S. Deng, Y. Chen, Y. Yang, C. Jin, ACS Nano **8**, 7130– 7137 (2014).

[38] Y. Gong, Z. Liu, A. R. Lupini, G. Shi, J. Lin, S. Najmaei, Z. Lin, A. L. Elias, A. Berkdemir, G. You, H. Terrones, M. Terrones, R. Vajtai, S. T. Pantelides, S. J. Pennycook, J. Lou, W. Zhou, and P. M. Ajayan, Nano Lett. **14**, 442– 449 (2014).

[39] Z. Lin, M. T. Thee, A. L. Elias, S. Feng, C. Zhou, K. Fujisawa, N. P. Lopez, V. Carozo, H. Terrones, and M. Terrones, Appl. Phys. Lett. Mater. **2**, 092514 (2014).

[40] Y. Chen, J. Xi, D. O. Dumcenco, Z. Liu, K. Suenaga, D. Wang, Z. Shuai, Y.-S. Huang, and L. Xie, ACS Nano **7**, 4610– 4616 (2013).

[41] Y. F. Chen, D. O. Dumcenco, Y. M. Zhu, X. Zhang, N. N. Mao, Q. L. Feng, M. Zhang, J. Zhang, P. H. Tan, and Y. S. Huang, et al, Nanoscale **4**, 2833– 2839 (2014).

[42] A. Ramasubramaniam, Phys. Rev. B **86**, 115409 (2012).

[43] M. M. Ugeda, A. J. Bradley, S.-F. Shi, F. H. da Jornada, Y. Zhang, D. Y. Qiu, S.-K. Mo, Z. Hussain, Z.-X. Shen, and F. Wang et al, Nat. Mater. **13**, 1091– 1095 (2014).

[44] See Supplemental Material at () for the sample preparation, characterization, tip-induced band bending, and derivation of thermal broadening and its effects on STS measurements.

[45] K. F. Mak, M. Y. Sfeir, Y. Wu, C. H. Lui, J. A. Misewich, and T. F. Heinz, Phys. Rev. Lett. **101**, 196405 (2008).

[46] E. Y. Andrei, G. Li, and X. Du, Rep. Prog. Phys. **75**, 056501 (2012).

[47] A. Luican, G. Li, and E. Y. Andrei, Solid State Commun. **149**, 1151−1156 (2009).

[48] G. Li, and E. Y. Andrei, Nat. Phys. **3**, 623−627 (2007).

[49] G. W. Shim, K. Yoo, S. B. Seo, J. Shin, D. Y. Jung, I. S. Kang, C. W. Ahn, B. J. Cho, and S. Y. Choi, ACS Nano 8, 6655– 6662 (2014).

[50] Z. Y. Zhu, Y. C. Cheng, and U. Schwingenschloegl, Phys. Rev. B **84**, 153402 (2011).

[51] E Burstein, and S. Lundqvist, Tunneling Phenomena in Solids. Plenum Press: New York, 1969.

[52] C. Zhang, Y. Chen, A. Johnson, M.-Y. Li, L.-J. Li, P. C. Mendell, R. M. Feenstra, and C.-K. Shih, Nano Lett. **15**, 6494–6500 (2015).

[53] S. Choi, Z. Shaolin, and W. Yang, J. Korean Phys. Soc. **64**, 1550 (2014).

[54] V. Kaushik, D. Varandani, and B. R. Mehta, J. Phys. Chem. C **119**, 20136 (2015).

[55] L. Britnell, R. Ribeiro, A. Eckmann, R. Jalil, B. Belle, A. Mishchenko, Y.-J. Kim, R. Gorbachev, T. Georgiou, and S. Morozov, et al, Science **340**, 1311 (2013).

[56] A. Molina-Sanchez, and L. Wirtz, Phys. Rev. B **84**, 155413 (2011).

[57] H. Shi, H. Pan, Y.-W. Zhang, and B. I. Yakobson, Phys. Rev. B, **87**, 155304 (2013).

[58] R. M. Feenstra, J. Vac. Sci. Technol., B **21**, 2080 (2003).

[59] R. M. Feenstra, G. Meyer, and K.-H. Rieder, Phys. Rev. B **69**, 081309 (2004).

[60] R. M. Feenstra, S. Gaan, G. Meyer, and K.-H. Rieder, Phys. Rev. B **71**, 125316 (2005).

[61] A. Chernikov, A. van der Zande, H. M. Hill, A. F. Rigosi, A. Velauthapillai, J. Hone, and T. F. Heinz, Phys. Rev. Lett. **115**, 126802 (2015).

[62] M.-H. Chiu, C. Zhang, H. W. Shiu, C.-P. Chu, C.-H. Chen, C.-Y. S. Chang, C.-H. Chen, and M.-Y.Chou, et al, Nat. Commun. **6**, 7666 (2015).

[63] X. Liu, I. Balla, H. Bergeron, G. P. Campbell, M. J. Bedzyk, and M. C. Hersam, ACS Nano 2015, **10**, 1067-1075 (2016).

[64] C. Zhang, A. Johnson, C. L. Hsu, L. J. Li, and C. K. Shih, Nano Lett. **14**, 2443 (2014).

[65] K. Kosmider, and J. Fernandez-Rossier, Phys. Rev. B **87**, 075451 (2013).

[66] H. P. Komsa, and A. V. Krasheninnikov, Phys. Rev. B **88**, 085318 (2013).

[67] H.-L. Liu, C.-C. Shen, S.-H. Su, C.-L. Hsu, M.-Y. Li, and L.-J. Li, Appl. Phys. Lett. **105**, 201905 (2014).

[68] N. Peimyoo, J. Shang, C. Cong, X. Shen, X. Wu, E. K. L. Yeow, and T. Yu, ACS Nano **7**, 10985– 10994 (2013).

[69] I Kylänpää, and H. P. Komsa, Phys. Rev. B **92**, 205418 (2015).

[70] H. Chandrasekar, and D. N. Nath, Mater. Res. Express **2**, 095007 (2015).